

Light scattering by nonspherical particles: Application to coccoliths detached from *Emiliania huxleyi*

Howard R. Gordon¹ and Tao Du²

Department of Physics, University of Miami, Coral Gables, Florida 33124

Abstract

Computation of the light scattering properties of marine particles has typically been effected using Mie theory (i.e., modeling the particles as homogeneous or layered spheres). Because scattering by irregularly shaped particles is significantly different from that of spheres, particularly in backscattering directions, it is of interest to examine the efficacy of using more complex formulations of light scattering that are not limited to spherically symmetric particles. We applied the discrete dipole approximation (DDA) to the computation of the scattering properties of detached calcium carbonate coccoliths from the coccolithophorid *Emiliania huxleyi*. Three distinct models of *E. huxleyi* coccoliths were studied: thin disks with a diameter of approximately 2.75 μm , washers with a 1.38- μm hole in the disk, and two parallel disks joined by a hollow tube (a “fishing reel”). The model coccoliths all had the same volume (mass \approx 0.19 pg carbon) and disk diameter and a refractive index of 1.20 relative to water. DDA computations for randomly oriented model coccoliths showed that the total scattering cross section and its spectral variation are similar for each of the three particle shapes and agree well with measurements made in natural *E. huxleyi* blooms both on a per-coccolith and per-calcite concentration basis. The backscattering cross section and its spectral variation was found to be strongly dependent on particle morphology. This dependence was shown to be due to multiple reflections within the particle. Scattering and backscattering coefficients for volume-equivalent spheres were within a factor of two of those for the disklike models.

Since the mid-1950s, when Burt (1956) produced his famous light scattering diagram, relating the scattering efficiency of spherical particles to their size and refractive index, many researchers have attempted to use Mie theory (van de Hulst, 1957) to explain the light scattering properties of suspended particulate matter in natural waters. Studies in the 1960s and 1970s combined measurements of the particle size distribution with Mie theory to explain the observed scattering coefficient and volume scattering function in terms of the particle refractive index (Beardsley et al. 1970; Gordon and Brown 1972; Morel 1973; Kullenberg 1974). Even though few marine particles even remotely resemble homogeneous spheres, these studies were reasonably successful in explaining the shape of the forward lobe of the volume scattering function (scattering angle Θ less than 90°), and in relating the total scattering and absorption coefficients to the particle concentration and size distribution. Gordon and Brown (1972) found that this required using refractive indices ($m = m_r - im_i$, where the real part describes refraction and the imaginary part describes absorption) with m_r in the range 1.01–1.05 (relative to water) and $m_i \leq 0.01$. The nearness of m_r to that of water suggested that much of the observed scattering was due to organic matter (e.g., phyto-

plankton) (Carder et al. 1972). However, in the backward scattering direction ($\Theta > 90^\circ$), these efforts were less successful. Brown and Gordon (1974) showed that the only way to explain the backscattering, based on the part of the size distribution that they were able to measure (diameters, D , for volume-equivalent spheres $\geq 0.65 \mu\text{m}$), was for all particles in the size range $1.25 \leq D \leq 3.75 \mu\text{m}$ to be high-index minerals ($m = 1.15 - i0$). This seemed somewhat unlikely, although alternative explanations required rather drastic assumptions regarding the then-unobservable particles with $D \leq 0.65 \mu\text{m}$.

Following the seminal work of Morel and Bricaud (1981) in applying the anomalous diffraction approximation of Mie theory (van de Hulst 1957) to understanding the optics of phytoplankton, many investigators in the 1980s began to use Mie theory to explain the observed spectrum of phytoplankton absorption and scattering coefficients in terms of the their size and the spectrum of m (see Morel 1994 for a review).

Recently, Volten et al. (1998) presented measurements of volume scattering functions ($20^\circ \leq \Theta \leq 160^\circ$) for several different species of phytoplankton, with (more or less) spherical and cylindrical shapes. Using size distributions for volume-equivalent spheres (determined by Coulter Counter or microscope) and refractive indices (following Bricaud and Morel 1986), they employed Mie theory to compute volume scattering functions for comparison with the measurements. They found that the Mie calculations differed “significantly from the measured data” (p. 1193) in both the backscattering and the forward-scattering regions and that particles with similar morphologies can produce dissimilar scattering functions. In addition, internal structures such as gas vacuoles were seen to significantly affect scattering. They suggest it is time to apply computational methods that better address particle morphology.

¹ Corresponding author (hgordon@miami.edu).

² Present address: PicoNetics, Inc., 5020B Brandin Court, Fremont, California 94538.

Acknowledgments

The authors are grateful for support from the U.S. Office of Naval Research, Oceanic Optics Program, under grant N00014-99-1-0007. We also thank B. T. Draine and P. J. Flatau for providing the DDSCAT computer code, M. I. Mishchenko for providing us with the T-Matrix computations used for validation of our DDA computations, and W. M. Balch and K. J. Voss for clarifying questions regarding the experimental measurements.

The advent of ocean color remote sensing with the Coastal Zone Color Scanner rekindled interest in backscattering by suspended particles because the remotely sensed water-leaving radiance is proportional to the total backscattering coefficient divided by the total absorption coefficient (Gordon and Morel 1983). Thus, the backscattering coefficient is a key constituent property in remote sensing. This backscattering co-varies with the phytoplankton concentration (actually with chlorophyll *a*) but cannot be due to phytoplankton because Mie theory studies showed that they must have very low backscattering efficiencies. Suggestions for augmenting phytoplankton backscattering ranged from microscopic particles (bacteria and viruses) co-varying with phytoplankton (Stramski and Kiefer 1991), to submerged air bubbles (Zhang et al. 1998), to suspended calcite (Balch et al. 2001); however, no study has been able to explain successfully the backscattering of particles suspended in seawater. Thus, investigators working with ocean color remote sensing data are in the somewhat embarrassing position of not really knowing the source of their “signal.”

In all of the work described above, the marine particles were modeled as spheres. Usually the spheres were homogeneous. Some recent studies modeled particles as concentric spheres in which m was allowed to vary in the radial direction within the particle (usually assuming two values). Examples include a model for scattering from cells with a nucleus (Zaneveld and Kitchen 1995) and a model for scattering from submerged bubbles coated with a surfactant (Zhang et al. 1998). However, it is well known that scattering by irregularly shaped particles (even deviating only moderately from spheres) is significantly different from that of spheres, particularly in backscattering directions (Mishchenko and Travis 1994). In fact, in an early study of light scattering by nonspheres, Mugnai and Wiscombe (1989) suggested that in the context of light scattering, spheres are “the most unrepresentative shape possible—almost a singularity if you will” (p. 3071). Although Aas (1984) has developed formulas in the anomalous diffraction approximation for the scattering and absorption cross sections of randomly oriented long cylinders and thin disks that are valid when the index of refraction is close to unity, to our knowledge virtually no computations have been attempted for marine particles with more realistic shapes using rigorous electromagnetic scattering theory.

In this paper, we take the next logical step in marine light scattering studies by applying to marine particles a version of electromagnetic scattering theory that is capable of treating particles of arbitrary shape. The goal of the study is to see if including the additional complexity of shape in marine particle light scattering studies provides significant additional information over and above that obtained by modeling the particles as spheres. Knowing full well that it is impossible to completely capture the complex shapes of marine particles, we only examine the efficacy of modeling them with simple shapes that more closely resemble their actual appearance than spheres. A secondary goal is to examine the influence of particle morphology on light scattering.

We focus on computing the scattering properties of calcium carbonate coccoliths detached from the coccolithophorid *Emiliania huxleyi*. These detached coccoliths are well

suited for our study because (1) they have a reasonably well-defined shape that in the first approximation resembles a disk of known diameter; (2) their composition is known (calcium carbonate) so m is provided and not a free parameter, and (3) measurements of coccolith scattering and backscattering are available; thus, they are almost ideal objects with which to examine the possibility of modeling scattering by irregularly shaped marine particles with simple nonspherical shapes. In addition, *E. huxleyi* blooms are known to turn the water a milky white color that is easily observed from space by ocean color sensors (Holligan et al. 1983). The interpretation of this remotely sensed color change in *E. huxleyi* blooms requires knowing their backscattering properties in the visible (Gordon et al. 1988, 2001) and, especially, the red and near infrared regions of the spectrum. However, the backscattering properties have been measured only in the visible. If we can successfully model the backscattering properties in the visible, then we can reliably extrapolate the computations into the near infrared.

First, we describe our model for coccoliths. Then, we describe and validate the method we use for solving the electromagnetic scattering problem for these models. Next, we present the scattering computations for the modeled coccoliths and develop a simple interpretation of the spectral dependence of their backscattering. Finally, we compare the modeled scattering with field data.

Physical model used for detached coccoliths

A physical model of a coccolith consists of a particle size and shape (morphology) and a refractive index, m . A shape that roughly approximates a coccolith is a disk of diameter D ($\sim 2.75 \mu\text{m}$). Estimates of the mass of an individual coccolith have varied over a wide range. Balch et al. (1991) review the estimates that range from 0.065 (Linschooten et al. 1991) to 0.6 (Holligan et al. 1983) pg C coccolith⁻¹, and adopt a value of 0.2 pg C coccolith⁻¹ for *E. huxleyi*. The density of calcite is 2.71 g cm⁻³, which suggests a volume of 0.616 μm^3 . We adopted this as the volume of our model coccolith; however, because of a computational error, a coccolith volume of 0.587 μm^3 was actually used. This corresponds to a mass of 0.191 pg C coccolith⁻¹, still well within the range of the estimates. Using this volume, the thickness of the model coccolith is 0.098 μm . This is the simplest approximation to the coccoliths of *E. huxleyi*.

Examination of Fig. 1 suggests that somewhat more complex morphologies may better approximate coccoliths. First, the coccoliths have a circular portion at the center that is very thin, suggesting that a more appropriate shape may be a disk with a circular hole centered on the disk (i.e., a “washer”). Most coccoliths appear to resemble two disks parallel to one another joined at the center (in the vicinity of the hole in the washer). This geometry looks like a fishing reel. We modeled coccoliths using these three shapes in the dimensions shown in Fig. 2. In each case, the diameter of the disk and the hole was determined by visually examining the electron microscope images. The thickness of the disk(s) was then chosen to make the coccolith volume 0.587 μm^3 , except for the fishing reel, where the disks were chosen to

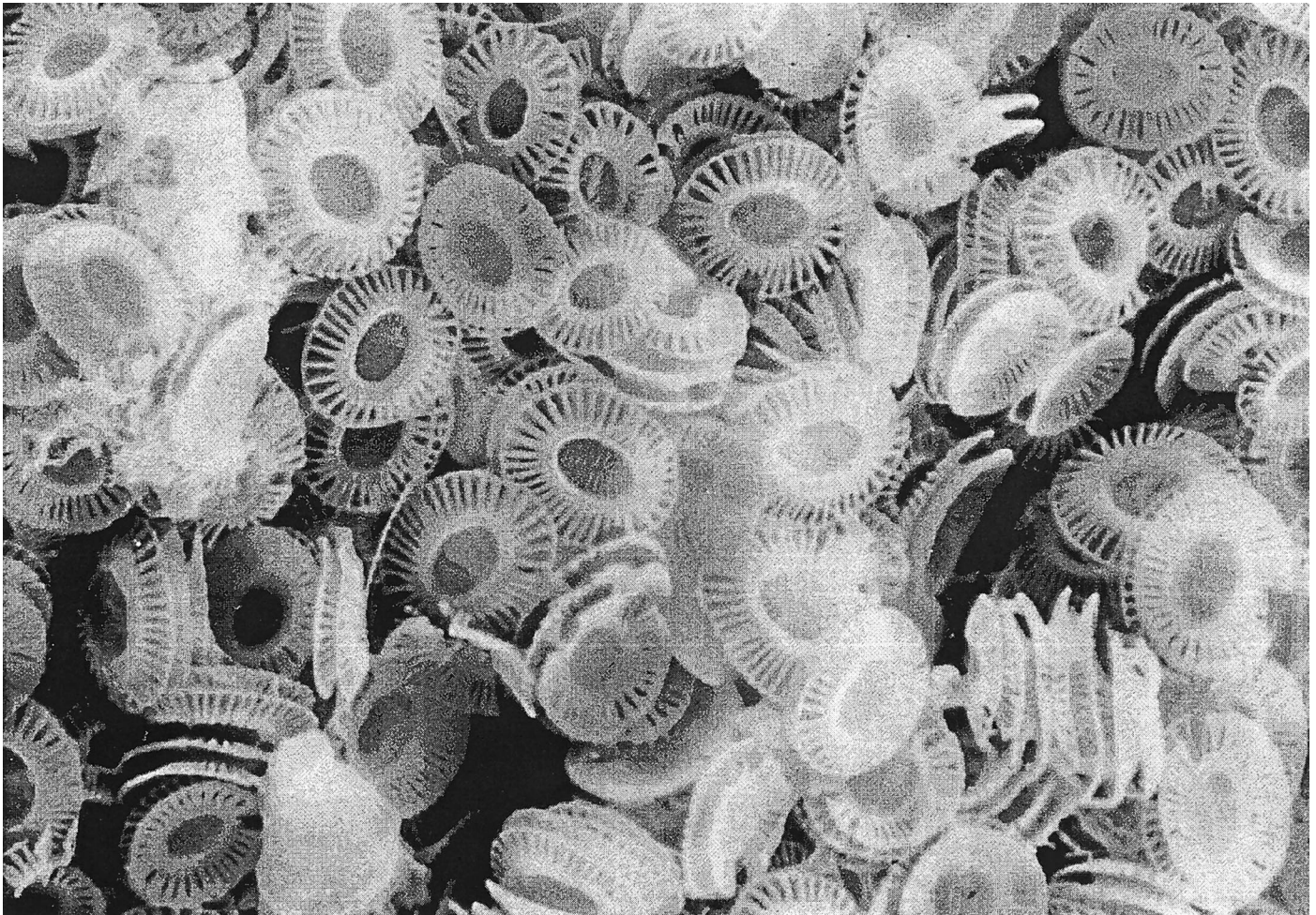


Fig. 1. Photograph of *E. huxleyi* detached coccoliths. The individual coccoliths are approximately $2.75 \mu\text{m}$ in diameter. (Photo courtesy of W. M. Balch.)

be $0.05 \mu\text{m}$ thick and separated by $0.10 \mu\text{m}$. The volume was then forced to be $0.587 \mu\text{m}^3$ by choosing the appropriate thickness of the reel joining the two disks. Thus, all three particle morphologies yielded a model coccolith with the same diameter and volume (mass).

Calcite is a birefringent (uniaxial) crystal; that is, its refractive index depends on the direction (and polarization) of propagation of light relative to a unique crystal direction, the optic axis. Young et al. (1992) studied the crystal assembly of coccoliths and concluded that the individual *E. huxleyi* coccoliths are composed of calcite crystals with their optic axis (the *c*-axis) in the radial direction. For the individual coccoliths in Fig. 1, the optic axis is parallel to the structures that resemble the spokes of a wheel. Thus, our model coccoliths—disk (D), washer (W), and fishing reel—should be birefringent with the optic axis in the radial direction. However, although some formulations of the electromagnetic scattering problem are applicable to birefringent particles (Bohren and Huffman 1983), none are available for dealing with anisotropies as complex as this. An approximation is necessary to make the model tractable. We approximate the refractive properties by the mean refractive index (defined

as the speed of light in vacuum divided by the speed of light in the crystal) averaged over all directions of propagation (and all polarizations) relative to the optic axis. This turns out to be $\frac{2}{3}$ of the “ordinary” index plus $\frac{1}{3}$ of the “extraordinary” index (Aas 1981). For vacuum wavelengths from 400 to 700 nm, this yielded $m = 1.214$ to 1.197 relative to water, with an average of 1.203. Our model assumes that the index is 1.20 and independent of wavelength. This is close to the value of 1.19 given by Aas (1981).

The electromagnetic scattering problem

Van de Hulst (1957) and Bohren and Huffman (1983) discuss methods of light scattering computations for spherical particles in detail. Reviews of recent work in light scattering by nonspherical particles are presented in Mishchenko et al. (2000).

Traditionally, the scattering by irregularly shaped particles has been approximated by the scattering by spherical particles having the same volume or surface area. However even for smooth particles, such as ellipsoids with aspect ratios less than two, the scattering by area-equivalent spheres is signif-

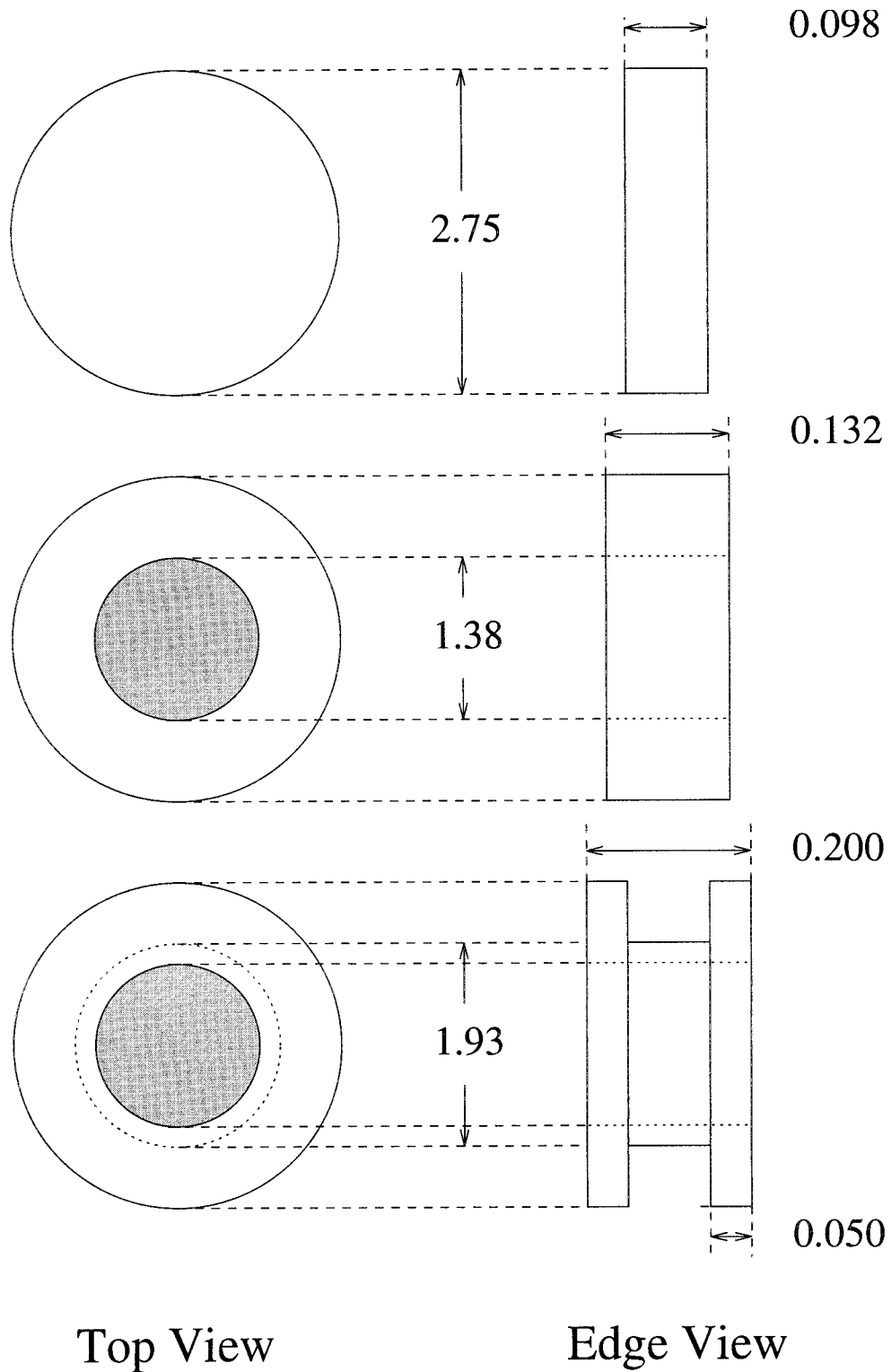


Fig. 2. Schematic of the three models for coccoliths: top is the disk, middle is the washer, and bottom is the small fishing reel. All dimensions are in μm .

icantly different from that of the actual particle (*see, e.g.,* Mishchenko and Travis 1994). For particles with simple shapes such as ellipsoids and cylinders, the most successful approach to light scattering is the so-called “T-Matrix”

method as formulated by Mishchenko and Travis (1994). This method is similar to Mie theory in that it provides an exact solution; however, computational difficulties prevent its application to arbitrarily large particles. An important fea-

ture of the Mishchenko and Travis computer code is that it analytically averages over particle orientation. This allows straightforward computation of scattering from suspensions of randomly oriented particles. The code is described in detail (along with limitations) in Mishchenko and Travis (1998). Unfortunately, it has not been formulated for the more complex shapes employed here (the washer and the fishing reel). The only method to compute electromagnetic scattering from arbitrarily shaped particles is the so-called discrete dipole approximation (DDA) formulated by Purcell and Pennypacker (1973).

The physical basis of the DDA can be understood by considering the light scattering process, beginning with scattering from a small dielectric sphere. When such a sphere is illuminated by an electromagnetic (EM) wave with $\lambda \gg$ the diameter, all portions of the sphere essentially will be subjected to the same oscillating electric field. (There will be no spatial variation of the field over the particle, only a temporal variation.) This field will induce a dipole moment in the sphere that is proportional to the electric field (a process called polarization). The induced dipole moment will oscillate in phase with the field and radiate EM waves in all directions with the same frequency and phase as the incident wave. This field viewed at a great distance from the sphere (the “far field”) is the scattered radiation. This is called Rayleigh scattering.

As the sphere’s size increases relative to λ , individual portions of the particle will no longer be subjected to the same field at any instant of time (a spatial variation of the field will exist over the sphere). This field induces a dipole moment that varies with position and oscillation phase within the sphere. The EM far field induced by the oscillating dipole moments of the various portions of the sphere will interfere in the far field constituting the scattered radiation. Because the dipole moments of the individual portions are no longer in phase (as they are for a very small particle), the scattering will differ from Rayleigh scattering. If the EM field, to which each portion of the particle is subjected, is approximated by the incident EM field alone, the result is termed Rayleigh–Gans scattering (van de Hulst 1957). Conversely, if each portion of the particle is subjected to the true EM field (the incident field *plus* the field generated by all other portions of the sphere), the resulting far field provides an *exact* solution to the scattering problem. The DDA is a discrete formulation of this exact solution in which the particle is composed of a cubic lattice of N polarizable dipoles with the lattice boundaries approximating the boundary of the particle. The dipoles represent the individual portions of the particle in the preceding discussion. Clearly, particles of any shape can be represented in this manner with a sufficiently large N . This method was further developed by Draine (1988) and Draine and Flatau (1994), resulting in the freely distributed program DDSCAT (<http://www.astro.princeton.edu/~draine/DDSCAT.html>). We used this code for the computations described here.

The DDA provides the differential scattering cross section $d\sigma(\Theta)/d\Omega$, where Ω is the solid angle and Θ is the scattering angle. The total scattering cross section, σ , and the backscattering cross section, σ_b , are given by

$$\sigma \equiv 2\pi \int_{\Theta=0}^{\Theta=\pi} \frac{d\sigma(\Theta)}{d\Omega} \sin \Theta \, d\Theta, \quad \text{and}$$

$$\sigma_b \equiv 2\pi \int_{\Theta=\pi/2}^{\Theta=\pi} \frac{d\sigma(\Theta)}{d\Omega} \sin \Theta \, d\Theta,$$

respectively. The scattering phase function is defined by $P(\Theta) \equiv d\sigma(\Theta)/\sigma dV$, and the usual volume scattering function of marine optics, $\beta(\Theta)$, is the differential scattering cross section *per unit volume* of scattering medium. Thus, the contribution that particles of a given size and shape make to the total scattering coefficient (b) and backscattering coefficient (b_b) is $b = n\sigma$ and $b_b = n\sigma_b$, where n is the number density of such particles.

Of the three wavelengths in the scattering problem, we will consider the vacuum wavelength λ first. This is the wavelength of the radiation measured in a vacuum (or in practice, in air) and is the wavelength usually reported in scattering experiments. Next is the wavelength in the medium surrounding the particle, λ_{Med} . In our case, the medium is water, and $\lambda_{\text{Med}} = \lambda/m_{\text{Water}}$, where m_{Water} is the refractive index of water (~ 1.334). Finally, there is the wavelength of the radiation within the particle, λ_{Part} . This is used later in the analysis and is given by $\lambda_{\text{Part}} = \lambda/m_{\text{Part}} = \lambda_{\text{Med}}m_{\text{Water}}/m_{\text{Part}}$. In our computations, $m_{\text{Water}}/m_{\text{Part}} = (1.20)^{-1}$. We will also use the term wavelength or the symbol λ when the distinction regarding the medium is unimportant.

There are several important parameters in the DDA: d , the lattice spacing between the individual dipoles; k , the wave number ($k = 2\pi/\lambda_{\text{Med}}$); a_e , the radius of a spherical particle having the same volume V ($V = 4\pi a_e^3/3$); and N , the total number of dipoles used to represent the particle. A criterion for accurate computation of the scattering properties is $mkd < 1$ ($m = m_{\text{Part}}/m_{\text{Water}}$), with the computations improving as mkd decreases below unity. For a simply shaped object (e.g., a cube) this implies that $N > (mk)^3V$. The quantity ka_e is a convenient dimensionless measure of the particle size. It is similar to the size parameter in Mie theory. The DDA has been shown to provide accurate scattering cross sections (error of $< 2\%$) for values of ka_e as high as 20, with $mkd \approx 1$ (Draine 2000). However, with $mkd \approx 1$ the error in the scattering phase function can be large, particularly at scattering angles where the phase function itself is small. For most of our computations of model coccoliths, $V = 0.587 \mu\text{m}^3$, for which $a_e = 0.52 \mu\text{m}$, and $\lambda \geq 0.4 \mu\text{m}$ ($\lambda_{\text{Med}} \geq 0.3 \mu\text{m}$). These parameters yield $ka_e \leq 10.9$, and $mk \leq 25.2 \mu\text{m}^{-1}$. Following Draine (2000), we expect that application of the DDA with $mkd \approx 1$ to the models proposed here should yield excellent values for the total scattering cross section, but there may be significant error in the phase function in the backward direction, where it is small. Increasing accuracy requires decreasing d . Unfortunately, the computation time rapidly increases with decreasing d ; thus, there is a trade-off between computational effort and accuracy.

The Draine (2000) examples refer to a single orientation of the particle. Here we assume the coccoliths are in random orientation. This requires orientational averaging of the associated cross sections. In the DDA, the orientational averaging is carried out by computing σ and σ_b for a large number (N_{Or}) of orientations and averaging them. Thus, in

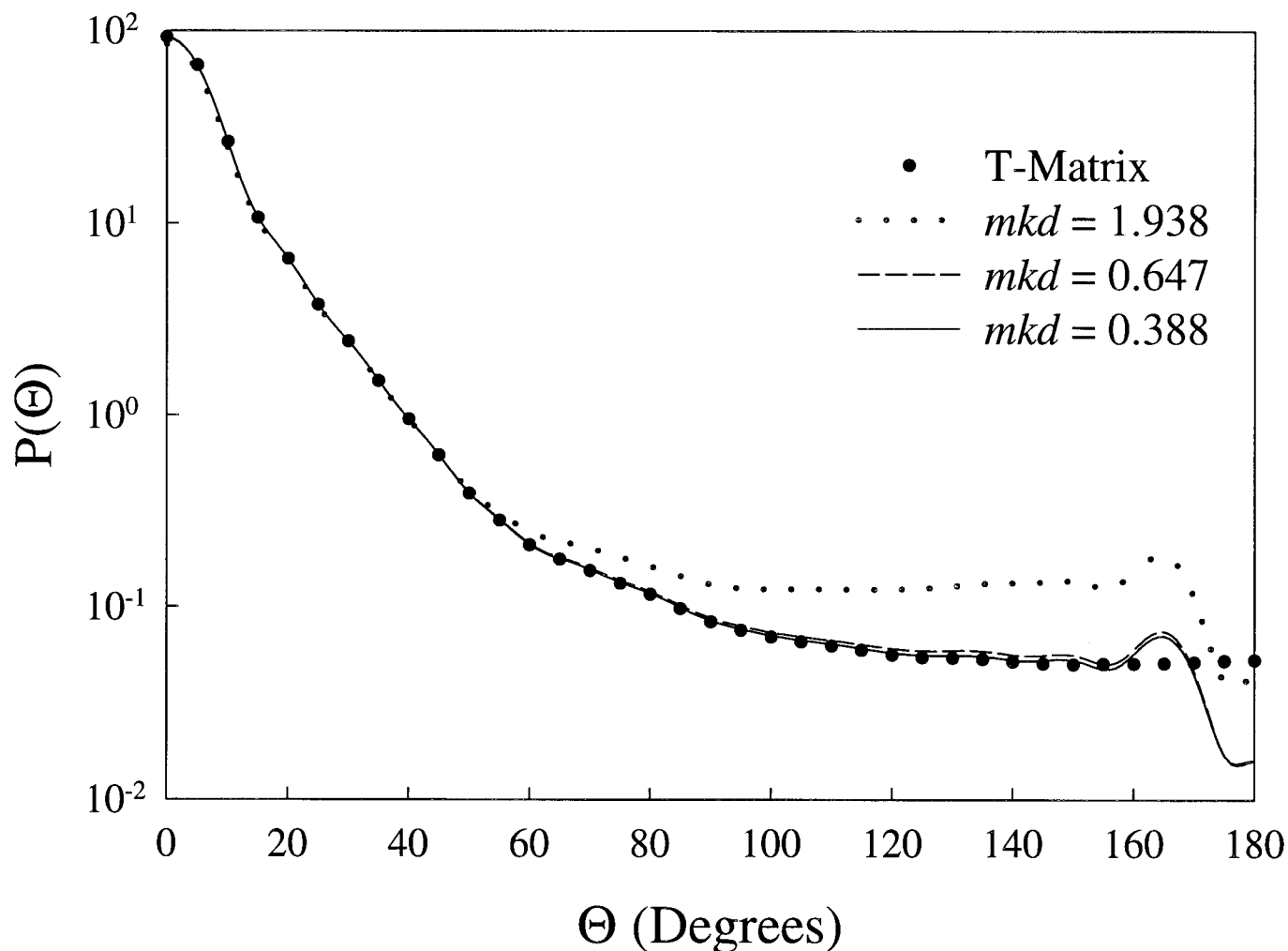


Fig. 3. Comparison of the scattering phase function at 700 nm for a disk with diameter 2.704 μm , thickness 0.1352 μm , and refractive index 1.20 relative to water computed using the T-Matrix method and the DDA with $N_{\text{Or}} = 5,049$. This shows the convergence of the DDA as the value of mkd decreases.

addition to requiring that mkd be sufficiently small, N_{Or} must be sufficiently large to provide accurate orientationally averaged cross sections. The computational burden is directly proportional to N_{Or} .

In fact, for a given particle shape and value of ka_e , acceptable values of d (or equivalently mkd) and N_{Or} must be determined by studying the convergence as a function of these parameters. That is, a set of computations must be carried out for a given particle in which mkd is decreased and N_{Or} is increased until the desired accuracy is achieved. In our cases, this is not practical because of the intense computational time associated with the DDA. However, for our simplest model (the disk) the T-Matrix method is available to test the DDA convergence. Mishchenko and Travis (1998) indicate that for $m = 1.311$, the T-Matrix method is capable of handling disks with an aspect ratio (diameter over thickness) up to 20 and a size parameter ($x_s = kr_s$, where r_s is the radius of the area-equivalent sphere) of seven. For smaller m , it is expected that larger cylinders can be treated. Thus, the T-Matrix can provide accurate cross sections for disks

sized similar to those of interest and can be used to determine acceptable values of mkd and N_{Or} .

Mishchenko kindly agreed to run the T-Matrix code at 0.7 μm for a disk with an index of 1.20, a diameter of 2.704 μm , and a thickness of 0.1352 μm . This disk is $\sim 35\%$ thicker than our disk model for the *E. huxleyi* coccolith and has $ka_e = 10.94$. We compared this computation with our operation of the DDA code for the same parameter values. In the comparison, orientational averaging in the DDA was carried out using $N_{\text{Or}} = 5,049$. This corresponds to (1) the angle between the normal to the disk and the incident beam assuming 51 values between 0 and 90° and (2) the azimuth of the normal around the incident beam assuming 99 values between 0 and 180°. Because of the symmetry of the disk, these angular ranges are all that is required for a complete orientational average.

The results of the T-Matrix–DDA comparison are provided in Figs. 3–5. Figure 3 compares the scattering phase function $P(\Theta)$ as a function of mkd for the DDA and the T-Matrix. The figure shows that $P(\Theta)$ computed by the DDA

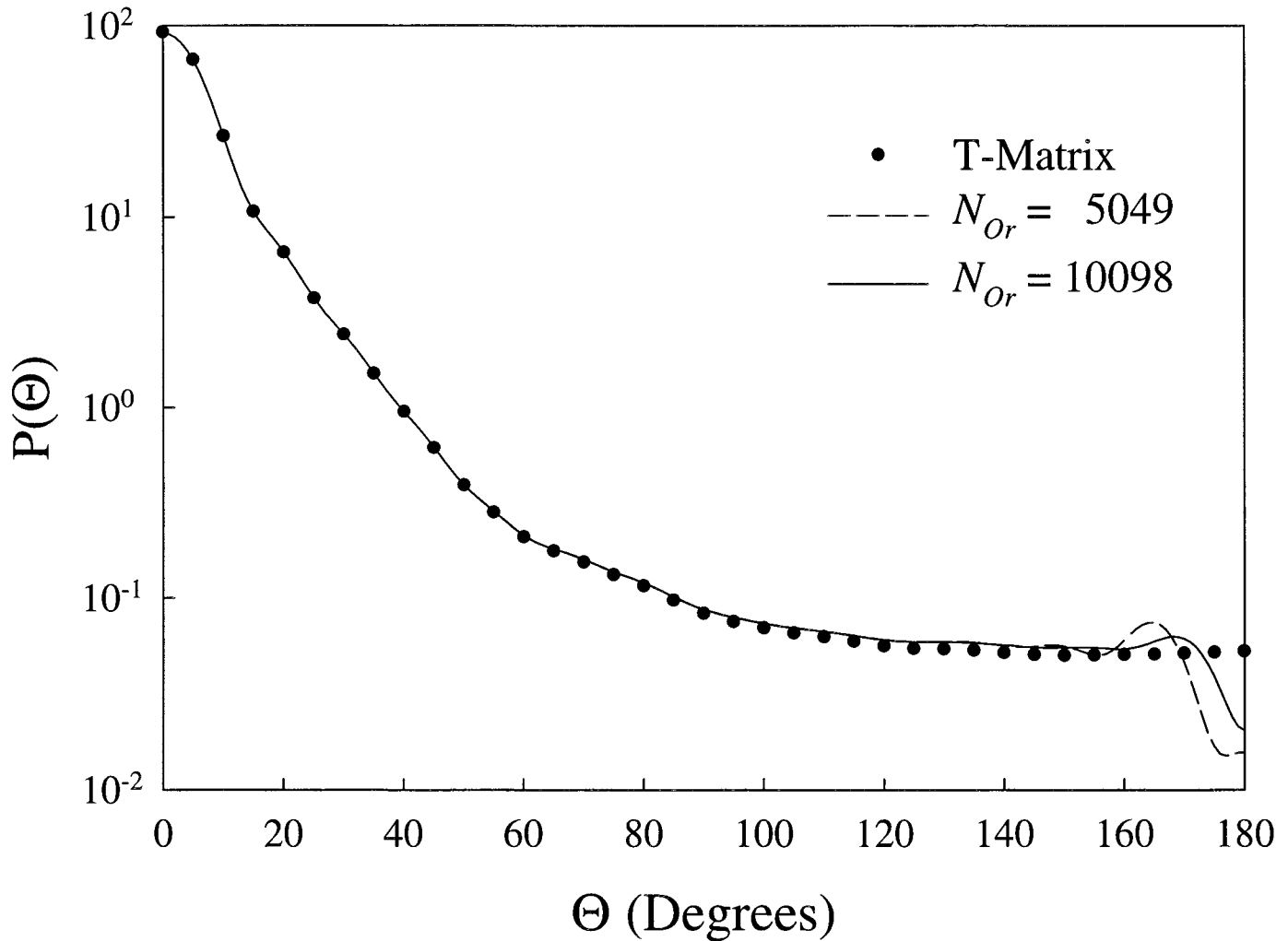


Fig. 4. Comparison of the scattering phase function at 700 nm for a disk with diameter 2.704 μm , thickness 0.1352 μm , and refractive index 1.20 relative to water computed using the T-Matrix method and the DDA with $mkd = 0.647$ and two values of N_{or} . This shows the effect of varying N_{or} in the DDA.

agrees well with the T-Matrix for scattering angles $< 90^\circ$. For larger angles, departures are seen, but as mkd decreases, the agreement improves. The large departure seen for $\Theta > 155^\circ$ is due to orientational averaging in the DDA. If the number of orientations is increased by letting the angle between the normal and the incident beam assume 102 values between 0 and 90° , better agreement is seen in the backward direction (Fig. 4). Figure 5 compares the DDA (as a function of mkd with $N_{or} = 5,049$) and T-Matrix computations of σ and σ_b . It shows that for $mkd \approx 0.65$, the errors for σ and σ_b are $\sim 2\%$ and $< 10\%$, respectively. For $mkd \approx 0.4$, the error in both is significantly smaller. Clearly, the orientational averaging error for $\Theta \geq 155^\circ$ produces little error in σ and σ_b . This owes to the $\sin \Theta$ factor in the integrals for σ and σ_b . This factor reduces the importance of scattering at large angles. Because the test disk is actually larger ($\sim 30\%$ in terms of volume) than our model coccoliths, we can expect that with similar values of mkd we can achieve similar accuracy in our DDA computations. A word of caution, however: the scattering phase functions computed using

these parameters cannot be accurate for $\Theta > 155^\circ$ because N_{or} is too small.

In the case of the fishing reel, computation time requires that we use mkd no smaller than ~ 0.63 at the shortest wavelength considered. Although the values of the parameters are close to those for which the error in σ and σ_b are $\sim 2\%$ and $< 10\%$, respectively, we wondered if the complex internal structure would influence the accuracy of the DDA. It is not feasible to reduce mkd further and carry out accurate orientational averaging; thus, to examine the accuracy in this case, we considered a single orientation: the plane of the fishing reel perpendicular to the incident (unpolarized) beam. Table 1 and Fig. 6 provide the results of this computation. Table 1 suggests that the errors in σ and σ_b will be similar to the error in the T-Matrix example described above. We see that the scattering phase function is not significantly different for mkd between 0.316 and 0.633, except in the near-backward direction. As discussed earlier, this region ($\Theta > 160^\circ$) contributes very little to σ or to σ_b .

In sum, this analysis suggests that we can expect that for

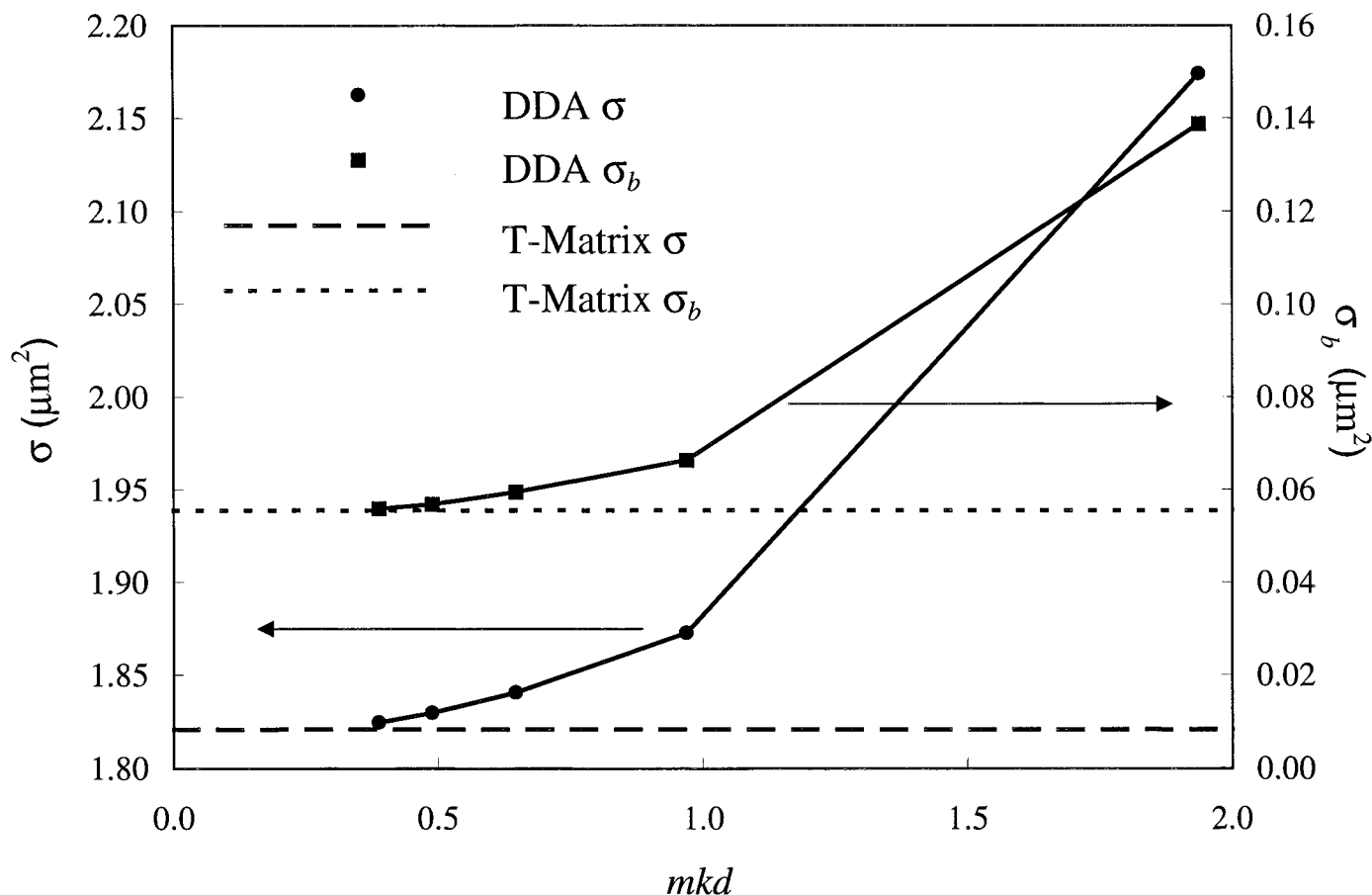


Fig. 5. DDA-computed scattering coefficient σ and backscattering coefficient σ_b as a function of mkd (with $N_{\text{or}} = 5,049$) showing the convergence of these quantities to the T-Matrix value (dashed lines) as mkd decreases.

the size of particle we are studying and the values of mkd ($\sim < 0.6$) and N_{or} (5,049) we are using, the DDA will yield σ and σ_b with an errors $< 2\%$ and $< 10\%$, respectively. The error in $P(\Theta)$ is likely to be large only for $\Theta > 155^\circ$.

Results of the scattering computations for model coccoliths

We computed the scattering by the model coccoliths in random orientation for the three shapes provided in Fig. 2 at $\lambda = 0.4, 0.5, 0.6, 0.7, 0.8,$ and $0.9 \mu\text{m}$. In addition, we examined two larger fishing reels for which the separation between the two disks was increased from 0.1 (SR) to 0.2 (MR) to $0.3 \mu\text{m}$ (BR), with the volume held constant by narrowing the thickness of the “reel” appropriately. The computational burden was intense: 58 d of CPU time on a DEC Server 2100 (200 MHz) were required for the first four

wavelengths of the small fishing reel (SR). For most of the computations, mkd ranged from ~ 0.28 at $\lambda = 900 \text{ nm}$ to 0.62 at $\lambda = 400 \text{ nm}$.

The total scattering cross section—The computed total scattering cross section of individual particles as a function of λ for the various models are provided in Fig. 7. We note that, for the disklike models, σ is only weakly dependent on the shape of the particle. Fig. 7 also shows that the spectral variation (500–900 nm) of σ is almost proportional to λ^{-2} , which is close to the dependence found by Voss et al. (1998) for detached coccoliths from *E. huxleyi* grown in cultures.

In addition to the four disklike shapes described above, we carried out computations for two spherical approximations to coccoliths: (1) a sphere with a volume equal to that of the model coccolith (radius $a_c = 0.519 \mu\text{m}$) and (2) a sphere with the same mean projected area as a disk with

Table 1. DDA results for the fishing reel oriented with the plane of the disk normal to the incident unpolarized beam.

N	4,736	37,600	126,888	300,832
mkd	1.253	0.6328	0.4189	0.3164
σ (μm^2)	14.439	14.479	14.445	14.429
σ_b (μm^2)	0.008658	0.006742	0.006069	0.006383

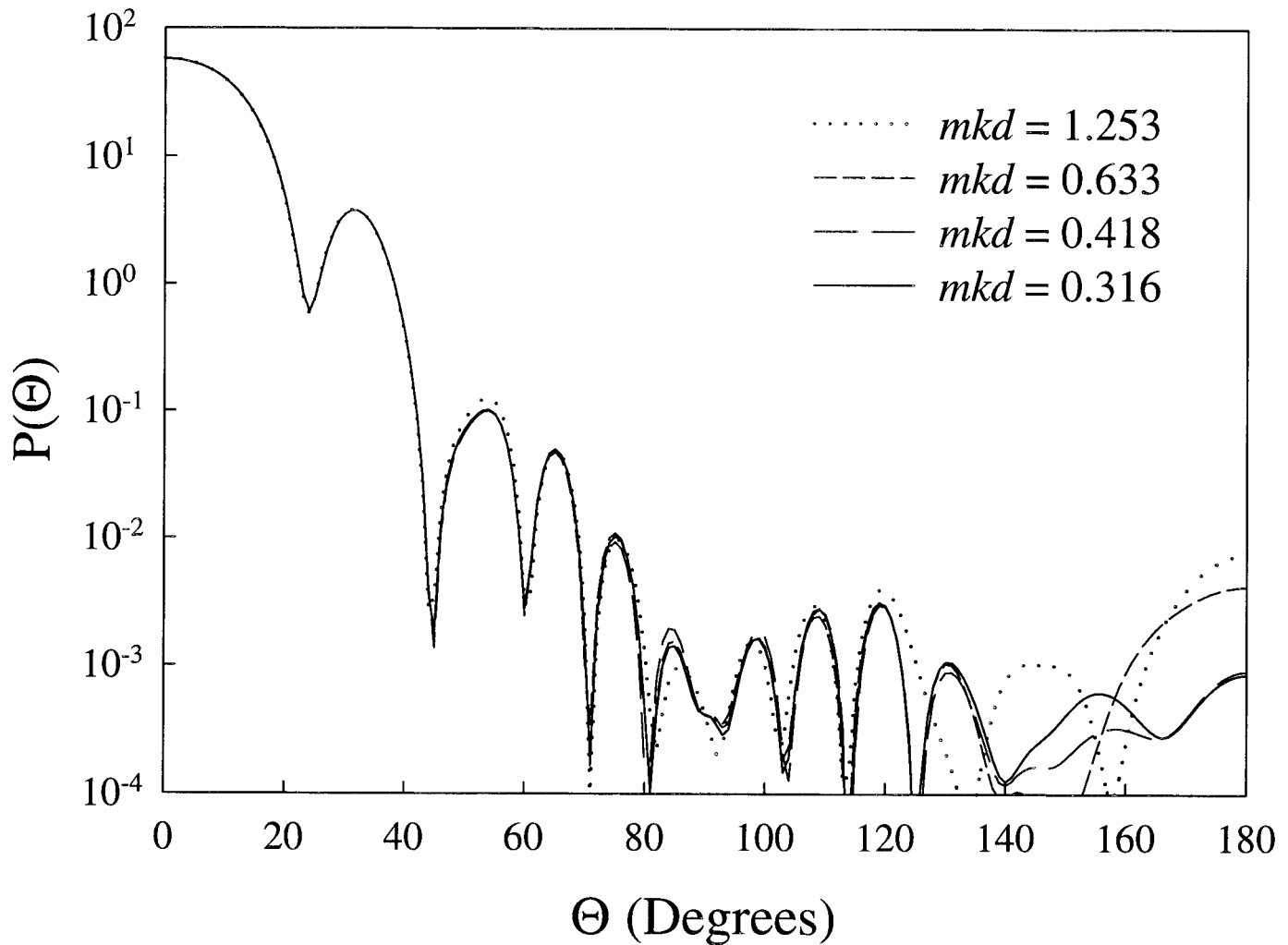


Fig. 6. Same as Fig. 3 for the small fishing reel oriented with the disk normal to the incident beam. This shows the convergence of the DDA as the value of mkd decreases.

diameter $2.75 \mu\text{m}$ (radius $a_\lambda = 0.972 \mu\text{m}$). In both cases, a narrow distribution of radii was used to smooth out the rapid oscillations present in Mie computations for monodisperse size distributions. The computations for the volume-equivalent sphere are included in Fig. 7. They show a weaker dependence on wavelength than the four model coccoliths ($\sigma \approx \lambda^{-1.46}$ from 600 to 900 nm) and larger scattering at all wavelengths. The computations for the mean projected area-equivalent sphere are not shown. This model leads to a much larger scattering cross section, with σ increasing from the blue to the red rather than decreasing ($5.34 \mu\text{m}^2$ at 400 nm and $11.06 \mu\text{m}^2$ at 800 nm). Clearly, the volume-equivalent sphere provides a better approximation to the scattering cross section of the disklike model coccoliths than the mean projected area-equivalent sphere. A sphere with the equivalent total area of the model coccoliths would yield an even larger scattering cross section.

The backscattering cross section—The computed backscattering cross sections σ_b are provided in Fig. 8. With the caveat that the computations in the blue (400 nm) may be

in error by approximately $\pm 10\%$ (because the smallest, $mkd \approx 0.62$, may be too large), they show a significant dependence on particle morphology—even in the very nature of the spectral dependence. The fishing reel models SR and BR show an increasing backscattering with decreasing wavelength for $\lambda \leq 600$ nm, whereas MR shows the reverse trend. Three of the five disklike models (D, W, BR) have similar behavior for $\lambda > 700$ nm, but a completely different behavior is seen for SR and MR. Within the context of the computations described, we are able to offer no explanation for this complex spectral behavior. There are no measurements in the near infrared to see which of the predicted spectral variations are realistic.

Additional model computations

The models described thus far were selected for their gross resemblance to coccoliths, subject to the constraint that their diameter be $2.75 \mu\text{m}$ and their mass 0.191 pg . However, because we are unable to explain the complex behavior of $\sigma_b(\lambda)$ shown in Fig. 8 for these models, we performed

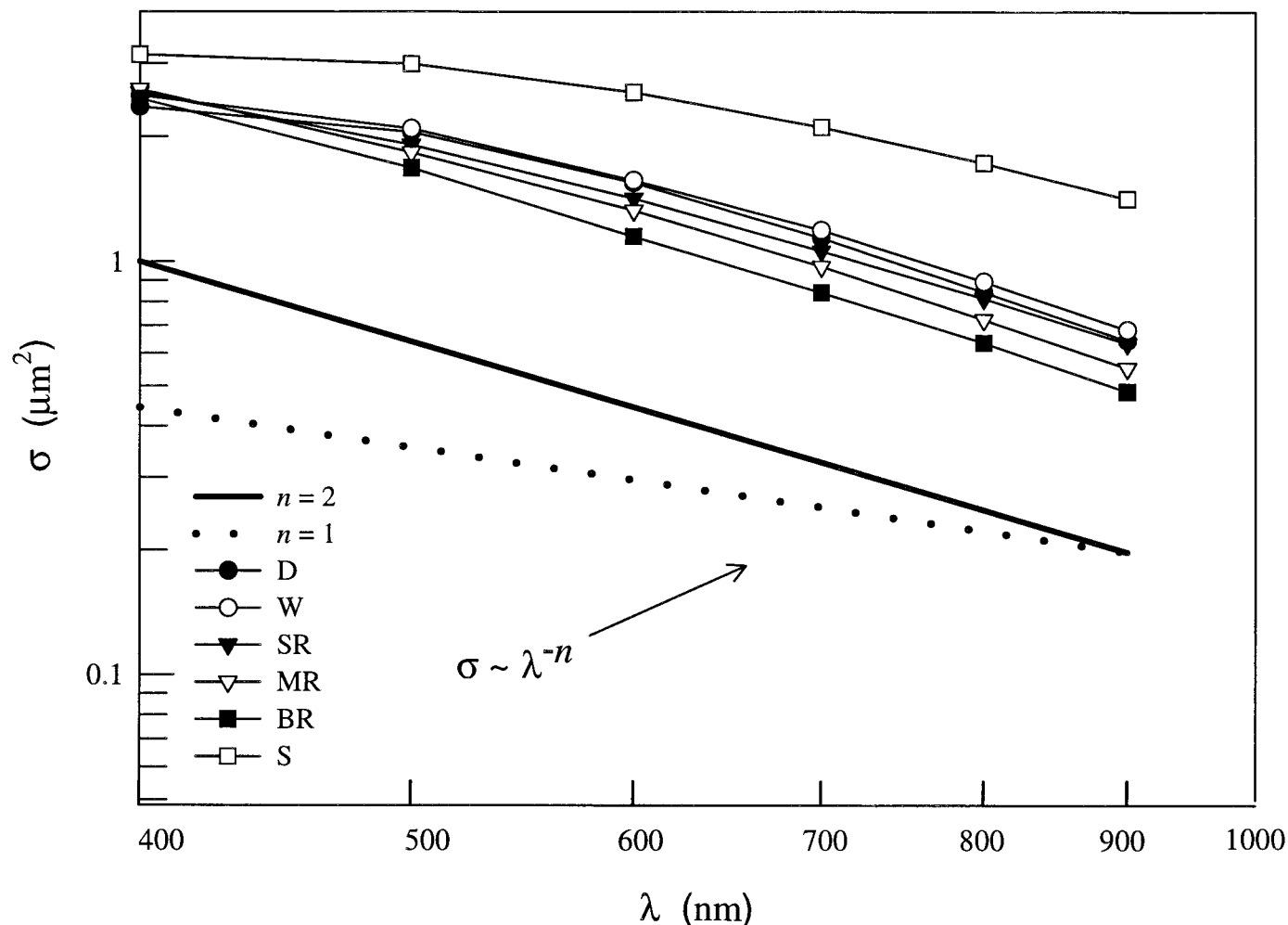


Fig. 7. Spectral variation of σ . D, disk model; W, washer model; SR, MR, and BR, the small, medium, and large fishing reels, respectively; S, volume-equivalent sphere. The two straight lines at the bottom are included for reference because they indicate a spectral variation $\sigma \approx \lambda^{-n}$ with $n = 1$ (dotted) and $n = 2$ (solid).

additional computations to try to develop an understanding of the spectral nature of the backscattering for these disklike objects. We believed that a reasonable starting point would be to try to understand $\sigma_b(\lambda)$ for disks and washers, the simplest of the shapes. We computed σ_b for disks and washers, where the thickness (t) was varied keeping the other dimensions as provided in Fig. 2. For disks, the results showed (Fig. 9) that for the various thicknesses, σ_b appeared to be very nearly a function of t/λ_{Med} alone; that is, disks of different thicknesses but with the same t/λ_{Med} had nearly the same σ_b . A similar result was obtained for the washer (Fig. 10). (Note that, were σ_b plotted as functions of t/λ_{Part} or t/λ , the scale on the x -axis would simply be stretched by a constant factor.) In addition, a set of computations for a smaller washer (an outer diameter of $2.50 \mu\text{m}$ but the same hole diameter of $1.38 \mu\text{m}$) showed that, at least qualitatively, this behavior is not dependent on D . The fact that $\sigma_b(\lambda)$ appears to reach a maximum near $t/\lambda_{\text{Med}} \approx 0.21$ or $t/\lambda_{\text{Part}} \approx 0.25$ (disk thickness $\frac{1}{4}$ of a wavelength of light *within* the disk) suggested that multiple reflections within the disk might play

a significant role in determining the spectral form of the backscattering.

To test the significance of internal reflections, we considered the reflection from an infinite flat plate of thickness t . Let $r(\psi)$ be the fraction of irradiance reflected from the plate when the radiation is incident at an angle ψ with respect to the normal to the plate. This reflected irradiance would have a scattering angle $\Theta = 180^\circ - 2\psi$, and the irradiance would be scattered into directions with $\Theta \geq 90^\circ$ as long as $\psi \leq 45^\circ$. When $\psi = 0$, $r(\psi)$ displays a series of maxima occurring when t is $\frac{1}{4}$ of the wavelength (in the plate), $\frac{3}{4}$ of the wavelength, and so on, and of minima when t is $\frac{1}{2}$ of the wavelength, one wavelength, and so on (Born and Wolf 1980). Thus, the first maximum in $r(\psi)$ occurs near the same value of t/λ_{Part} as the first maximum in σ_b .

We now model the backscattering from a disk by assuming that it reflects light in a manner similar to an infinite plate (i.e., according to $r(\psi)$ and Θ above); however, we ignore diffraction. This simply means that the individual light rays travel in straight lines within media and follow

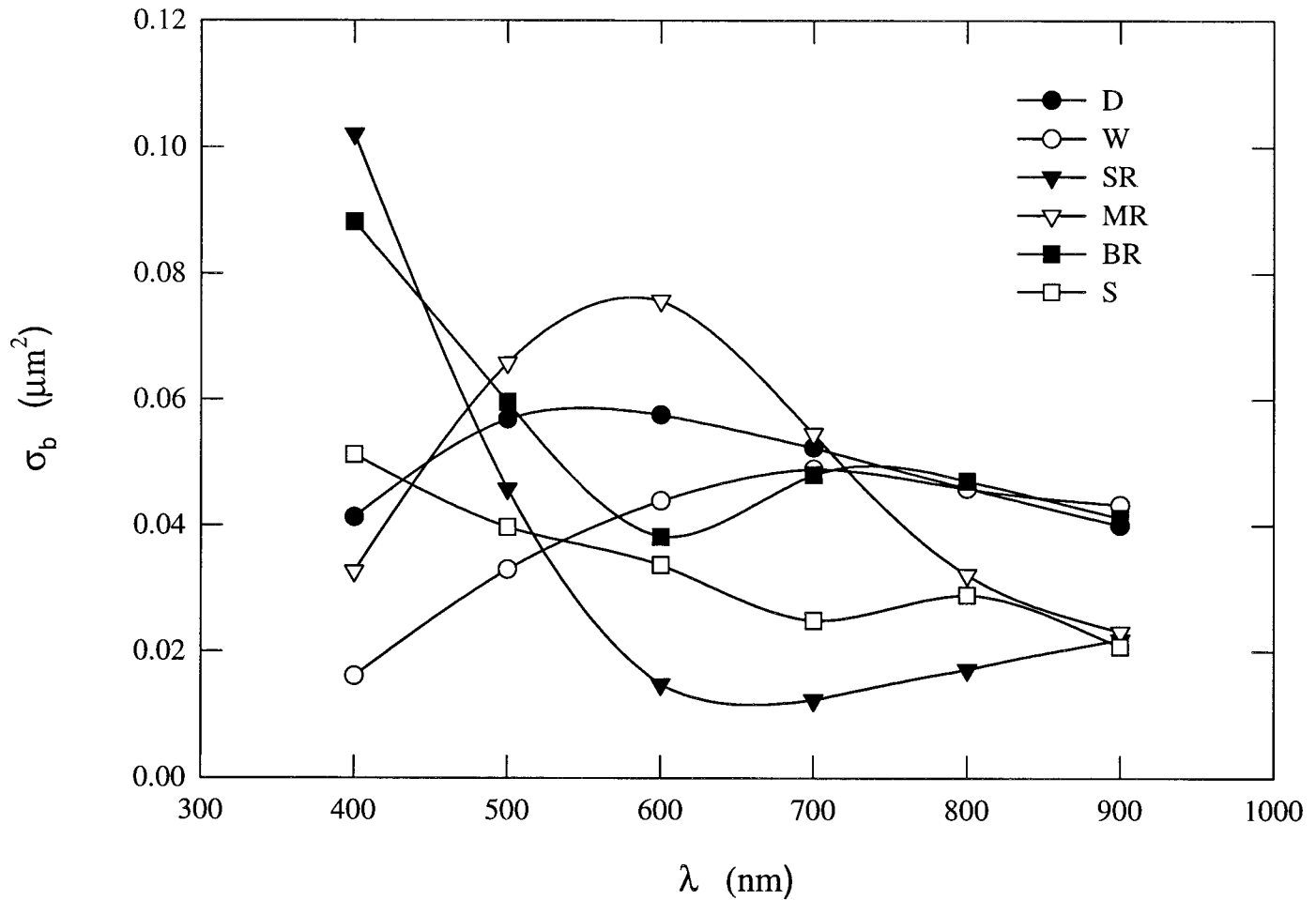


Fig. 8. Spectral variation of σ_b . Symbols are the same as Fig. 7.

Snell's law of refraction on striking either surface of the disk and that the various rays multiply reflected within the disk interfere on exiting. For a disk of area $A = \pi D^2/4$, the orientationally averaged backscattering cross section, Σ_b , is given by

$$\Sigma_b \equiv A \int_0^{\pi/4} r(\psi) \cos \psi \sin \psi \, d\psi.$$

Σ_b is thus the geometrical optics (with interference) approximation to the rigorously computed σ_b .

We computed Σ_b for a plate of thickness t and refractive index 1.2 relative to water as a function of t/λ_{Med} using the equations for $r(\psi)$ developed in Born and Wolf (1980). The results of this exercise are the solid lines in Figs. 9 and 10 (labeled "Plate"). (For the Fig. 10 computations, $A = \pi(D^2 - D_h^2)/4$, where D_h is the diameter of the hole.) The excellent agreement between Σ_b and σ_b shows that, within the size ranges we are considering, backscattering from (thin) disks and washers can be almost completely explained by multiple reflections within their structures. It should not be surprising that reflection from a disk with $t/D \ll 1$ would be similar to reflection from an infinite plate. However, when t becomes

a significant fraction of D , departures from the infinite plate model must occur, as seen in Figs. 9 and 10.

The success of this simple infinite plate model in explaining the spectral variation of σ_b for disks and washers suggests that we should try to model the more complex fishing reels in the same manner. We applied the Born and Wolf (1980) equations to compute Σ_b for an assembly consisting of two parallel plates of thickness $0.05 \mu\text{m}$ separated by 0.1, 0.2, and $0.3 \mu\text{m}$ to simulate the small, medium, and large fishing reels, respectively. The area A was chosen in the same manner as the washer. These computations are presented in Fig. 11. Comparison with Fig. 8 shows that multiple reflections between and within the plates of the fishing reels explain the peculiar spectral variation of their backscattering. In addition, it is seen that where σ_b is large (e.g., 400 nm for the small and medium fishing reels), Σ_b and σ_b are in quantitative agreement (within $\pm 13\%$ at the largest σ_b). In contrast, when σ_b is small (e.g., $\lambda > 600$ nm for the small fishing reel), Σ_b is significantly smaller than σ_b . We attribute this behavior to the scattering contribution from the structure (Fig. 2) holding the two disks in place (confirmed by additional computations not presented). Such scattering is apparently of minor importance when σ_b is large.

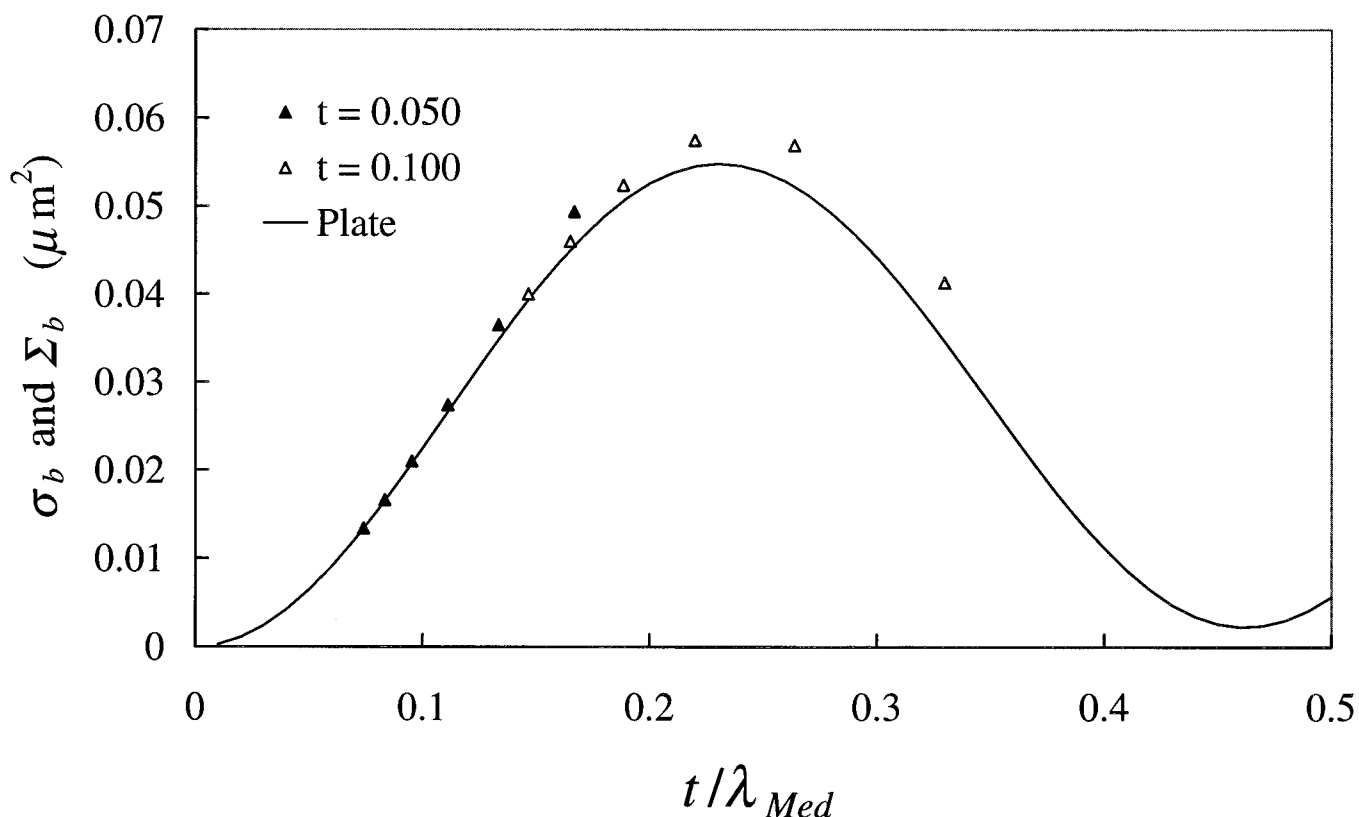


Fig. 9. Comparison between σ_b (symbols) and Σ_b (line) for disks with $D = 2.75 \mu\text{m}$ as a function of the thickness (t , μm) of the disk.

It is remarkable that such a simple model can explain the backscattering properties of such complex structures.

Influence of polydispersion

The computations thus far apply to systems in which the particles are monodisperse (i.e., all have the same shape and dimensions). Although, Fig. 1 suggests the dispersion in size and shape is actually small, it is certainly present. The main barrier to examining polydispersion is the heavy computational burden required. The success of the relatively simple model for σ_b (i.e., Σ_b for the size of disks and washers that we have been examining) allows us to overcome the computational barrier in the case of backscattering (at least for the disk and washer).

Consider disks or washers in which all of the dimensions are distributed in size. Let $dN(D, D_h, t)$ be the number of particles in a volume V with D between D and $D + dD$, D_h between D_h and $D_h + dD_h$, and so on. The size frequency distribution is defined by

$$n(D, D_h, t) = \frac{dN(D, D_h, t)/N_T}{dDdD_h dt},$$

where $N_T = \iiint dN(D, D_h, t)$ is the total number of particles in V . Then the backscattering cross section is

$$\sigma_b(\lambda) = \iiint n(D, D_h, t) \Sigma_b(D, D_h, t, \lambda) dD dD_h dt,$$

and the backscattering coefficient is $b_b(\lambda) = \sigma_b(\lambda)N_T/V$. These equations should provide reasonable estimates for σ_b and b_b as long as the distributions in D and D_h are not too wide (i.e., so the plate model is still valid).

We have applied this to a distribution of disks with $D_h = 0$; D and t uniformly distributed around means of 2.75 and 0.10 μm , respectively; and distribution widths of 0.5 and 0.05 for D and t , respectively. These are wider than would be suggested by Fig. 1. The resulting $\sigma_b(\lambda)$ is practically indistinguishable from that for a monodisperse distribution with the mean sizes. Thus, we do not think that limiting our discussion to monodisperse suspensions of disks and washers leads to significant error.

We can also consider polydispersion in the fishing reels by adding the spacing between the plates, t_{Gap} , to the argument list in dN and integrating over this variable. Figure 11 suggests that this would have a profound influence on the spectral dependence of σ_b . However, because the approximation Σ_b for σ_b considerably underestimates σ_b when Σ_b is small, we can expect that such results would provide only a qualitative estimate of the influence of dispersion in t_{Gap} .

The influence of polydispersion on the total scattering cross section will be discussed later.

Comparison with measurements

The disklike models appear to perform well in capturing the spectral variation of σ (i.e., $\sigma \approx \lambda^{-2}$); however, the spec-

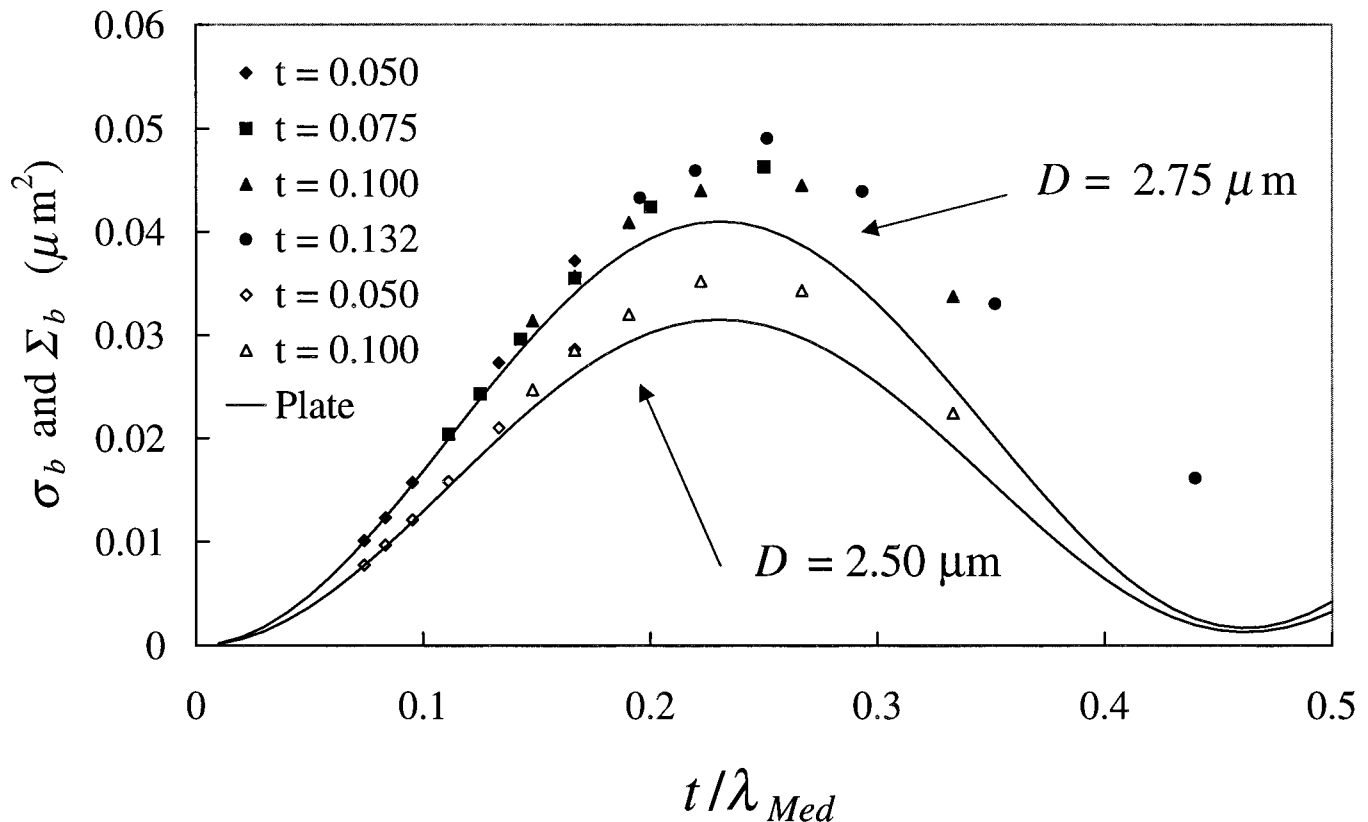


Fig. 10. Same as Fig. 9, but for washers. Open symbols are for $D = 2.50 \mu\text{m}$, solid symbols for $D = 2.75 \mu\text{m}$. t is in μm .

tral variation of σ_b is strongly dependent on morphology. There are sufficient measurements of σ and σ_b , both as functions of coccolith concentration and calcite concentration, for a quantitative comparison with our computations, and we make such a comparison in this section.

The total scattering coefficient—Table 2 compares σ at 550 nm with measurements. Note that the Balch et al. (1991) measurements were from a natural bloom (in the Gulf of Maine), whereas the Voss et al. (1998) measurements were on cultures. Unfortunately, the *E. huxleyi* measurements by Volten et al. (1998) are not applicable in this context, because the coccoliths were *attached* to the cells. Although the agreement with the natural bloom measurements is excellent, there is significant disagreement with the cultures. It is possible that the disagreement with Voss et al. (1998) for detached coccoliths of *E. huxleyi* grown in cultures could be due to the coccolith mass we used (0.191 pg C). Table 3 provides estimates of the mass of individual coccoliths made by several investigators. We note that the estimated mass varies by a factor of ~ 10 from low to high. For a limited number of cases, we varied the volume of the modeled coccoliths by varying the thickness of the disk(s) and diameter of the washer's hole. Figure 12 shows the resulting σ values at 700 nm as a function of the volume of the modeled coccolith. It suggests that, for the shapes we have employed, σ is roughly a linear function of the coccolith volume and, therefore, the coccolith mass. We converted the mass estimates in Table 3 to volume estimates using $V = 3.07m$,

where V is the volume (μm^3) and m is the mass (pg C). Then using Fig. 12, we estimated the corresponding σ at 700 nm and converted it to σ at 550 nm assuming $\sigma \sim \lambda^{-2}$ (Fig. 7; Voss et al. 1998). The resulting range in σ at 550 nm was $\sim 0.3\text{--}6.5 \mu\text{m}^2$, which covers the range of measurements summarized in Table 2. Thus, the disagreement with Voss et al. (1998) could be due to our choice of $0.587 \mu\text{m}^3$ for the coccolith volume.

Figure 12 also compares the DDA-derived σ s with those computed for thin disks of varying thickness (t) and fixed diameter ($2.75 \mu\text{m}$) using the approximate anomalous diffraction first-order expression derived by Aas (1984). The Aas formula, which should be valid when the parameter $\rho \equiv (m - 1)kt \ll 1$, slightly underestimates σ for disks up to a volume of approximately $1 \mu\text{m}^3$ and overestimates it for larger volumes. This simple formula also works reasonably well over the same range for the other shapes used in this study. These calculations show that for $D = 2.75 \mu\text{m}$, the Aas formula can be used to accurately compute σ up to $t = 0.2 \mu\text{m}$ or $\rho \approx 0.5$, unexpectedly close to unity. The validity of this formula explains the observed spectral dependence of σ (i.e., $\sigma \propto \rho^2 \propto k^2 \propto \lambda^{-2}$). Unfortunately, the anomalous diffraction approximation cannot be extended to estimate σ_b .

The Aas formula can also be used to examine the influence of polydispersion on σ in a manner similar to the plate models for σ_b . It is clear that for the small polydispersion to be expected for *E. huxleyi* coccoliths (Fig. 1), the spectral dependence of σ will not be altered from λ^{-2} , and the magnitude will be a weak function of polydispersion.

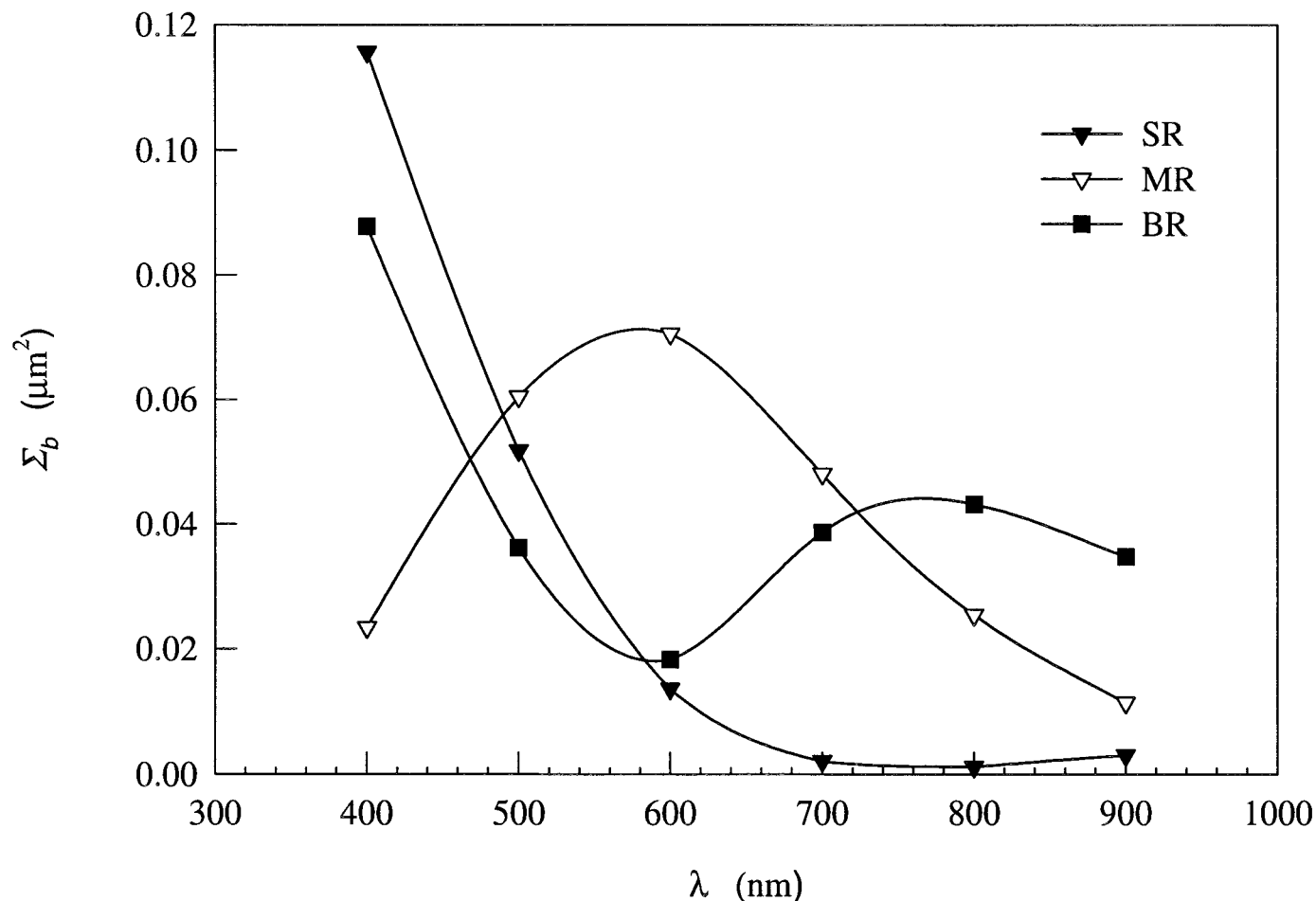


Fig. 11. Σ_b computed for the fishing reel models. Compare with σ_b in Fig. 8.

Some measurements relate coccolith scattering to calcite concentration $[\text{CaCO}_3]$ providing the calcite-specific scattering cross section $\sigma^* \equiv \sigma/[\text{CaCO}_3]$ and backscattering cross section $\sigma_b^* \equiv \sigma_b/[\text{CaCO}_3]$. These are compared with the disklike and spherelike models in Table 4. The Balch et al. (1996) measurements correspond to a natural bloom (North Atlantic 1991) at the highest concentrations of coccoliths compared to plated coccolithophores, so nearly all of the scattering was due to coccoliths. Clearly, the disklike models of coccoliths agree well with the measurements and provide a better approximation to σ^* at 550 nm than the sphere models. In sum, for both σ and σ^* , the disklike models agree with *field* measurements better than the sphere models.

Table 2. Computed and measured individual coccolith total scattering and backscattering cross sections at 550 nm.

Study	σ (μm^2)	σ_b (μm^2)
Disklike models	1.4–1.8	0.03–0.07
Sphere (equal volume)	2.8	0.036
Sphere (equal mean projected area)	7.6	0.24
Balch et al. (1991)	1.6	0.1
Balch et al. (1996)	—	0.135
Voss et al. (1998)	5.3	0.13–0.16

The backscattering coefficient—The magnitude and spectral variation of the computed σ_b and σ_b^* are compared with measurements in Tables 2, 4, and 5, respectively. The computed magnitudes of σ_b at 550 nm on a per-coccolith basis (Table 2) for the disklike models are a factor of two to four lower than the measurements. Figures 9 and 10 for the Σ_b approximation to σ_b suggest that in contrast to σ , increasing the volume above $0.587 \mu\text{m}^3$ for disks and washers with diameters near $2.75 \mu\text{m}$ will not increase σ_b . In fact, doubling the volume (by doubling t) will decrease σ_b significantly. The mean projected area-equivalent sphere model yields σ_b about a factor of two too large, and the volume-equivalent sphere is similar to the disklike models. On a per-calcite basis (Table 4) most models are satisfactory; however, they all provide too much backscattering.

Table 3. Estimates of coccolith mass.

Study	Mass (pg C)
Paasche (1962)	0.176
Linschooten et al. (1991)	0.065–0.078
Balch et al. (1991)	0.20
Balch et al. (1996)	0.47
Holligan et al. (1983)	0.6

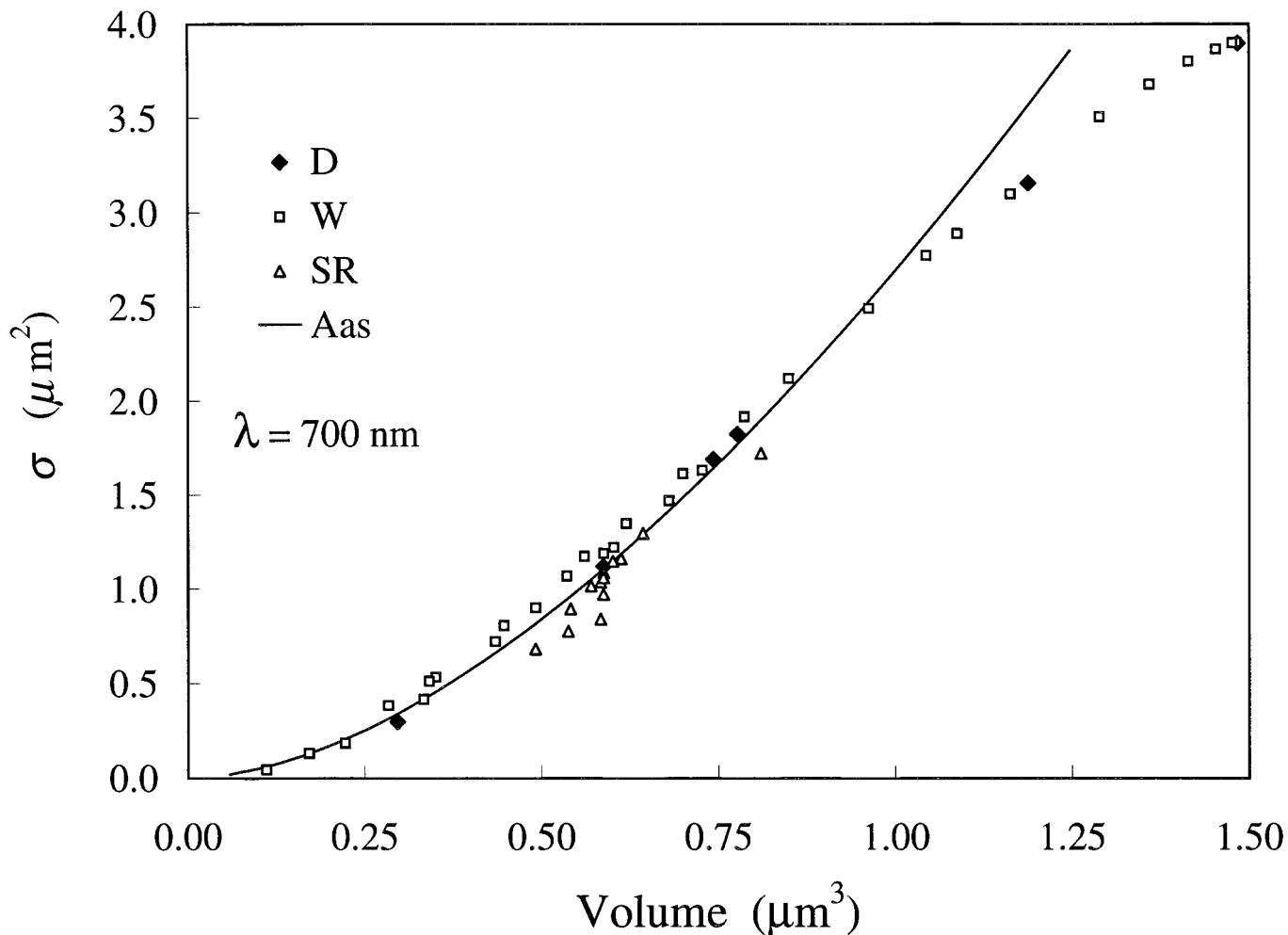


Fig. 12. Variation of σ with the volume of the pseudococcolith. These were computed by varying the thickness of the disk(s) in the three shapes and the diameter of the hole in the washer. The line is the Aas (1984) first-order anomalous diffraction result for thin disks [$\sigma \cong (\pi D^2/4)\rho^2 \ln(D/t)$, where D is the disk diameter, t is the disk thickness, and $\rho \cong (m - 1)kt$ computed by varying t and holding D fixed at $2.75 \mu\text{m}$].

Perhaps the most unsatisfactory part of this study is the poor performance of the disklike models in reproducing the spectral variation of σ_b . Disk and washer models with $t < \sim 0.05 \mu\text{m}$ (volume $< \sim 0.3 \mu\text{m}^3$) would provide nearly the correct spectral variation and correct values of σ^* and σ_b^* at 550 nm. However, for these dimensions, the values of σ and σ_b at 550 nm for individual coccoliths would be a factor of about two or three, or more, smaller than measured by Balch et al. (1991).

Table 4. The calcite-specific scattering and backscattering coefficients at 550 nm.

Study	σ^* ($\text{m}^2 \text{mol}^{-1}$)	σ_b^* ($\text{m}^2 \text{mol}^{-1}$)
Disklike models	88–113	1.9–4.4
Sphere (equal volume)	170	2.3
Sphere (equal mean projected area)	73	2.2
Balch et al. (1996)	101	1.6

A possibility for matching the spectral dependence and the values of the backscattering cross sections at 550 nm is to increase the disk diameter while simultaneously decreasing the thickness. We explored this for the disk (because of the simple dependence of σ_b , as approximated by Σ_b , on t and D). Noting that $\Sigma_b^* \cong \Sigma_b/[\text{CaCO}_3]$ depends only on the thickness of the disk (because both Σ_b and $[\text{CaCO}_3]$ are proportional to D^2), $t \cong 0.017 \mu\text{m}$ is required to provide $\Sigma_b^* \cong 1.6 \text{m}^2 \text{mol}^{-1}$ at 550 nm (Table 4). Keeping t fixed at this value, we varied D until $\Sigma_b \cong 0.1 \mu\text{m}^2$ (Table 2). This re-

Table 5. Computed spectral variation in backscattering cross section for modeled coccoliths.

Study	σ_b spectral variation
Present study	Very shape dependent
Balch et al. (1991)	λ^{-1}
Balch et al. (1996)	$\lambda^{-1.35}$
Voss et al. (1998)	$\lambda^{-1.40}$

quired $D \cong 13 \mu\text{m}$. Thus, we found that it was impossible to simultaneously match the field measurements of σ_b and σ_b^* (and their spectral dependence) with a single disk of realistic diameter. A similar result was obtained with the washer.

Considering the complex σ_b spectra seen for the fishing reel models, it is clear that the spectral dependence cannot be matched with a monodisperse suspension of any size reel. However, polydispersion of the fishing reel models could lead to spectra with the observed spectral variation. Therefore, polydispersion in t_{Gap} was also investigated as another possibility for reproducing the spectral variation of σ_b . Using the plate model (Σ_b) starting with the medium reel ($t_{\text{Gap}} = 0.2 \mu\text{m}$) and allowing t_{Gap} to be uniformly distributed over a range Δt_{Gap} , it was found that the spectral behavior of σ_b did not even decrease monotonically with increasing λ until $\Delta t_{\text{Gap}} \approx 0.18 \mu\text{m}$. This large value of Δt_{Gap} is not supported by Fig. 1.

It is interesting to observe that, for particles of the volume we have considered, the calcite-specific quantities show much less model-to-model variability in both σ and σ_b than the particle- or coccolith-specific quantities. Balch et al. (1999) also observed this behavior. They found that the species-to-species variability of σ_b for coccoliths formed by calcifying algae was approximately an order of magnitude less in the calcite-specific backscattering than in the coccolith-specific backscattering. In addition, our observation shows that approximating the particles by volume-equivalent or mean projected area-equivalent spheres can often lead to the correct order of magnitude for the mass-specific scattering quantities.

Concluding remarks

We have applied the DDA to compute the light scattering from disklike structures dimensioned to model *E. huxleyi* detached coccoliths. T-Matrix computations were used to validate our application of the DDA. Our results suggest that the total scattering coefficient of mineral marine particles can be adequately modeled by the DDA or any method that is capable of treating scattering from particles that approximate the shape of the particle in question. In fact, for the size range examined here, the first order of the anomalous diffraction approximation (Aas 1984) can be used to compute the total scattering coefficient and its spectral dependence. Furthermore, for σ , the precise shape of the particle is not necessary; however, approximating the disklike coccoliths as spheres is unsatisfactory. The volume-equivalent sphere yields at least 50% more scattering (per particle) than disklike particles, and the mean projected area-equivalent sphere yields as much as a factor of 10 too much scattering near 800 nm.

In regard to backscattering, although we can capture the observed $\sigma^*(\lambda)$ and $\sigma_b^*(\lambda)$ of coccoliths using simple disks and/or washers with volume $< \sim 0.3 \mu\text{m}^3$ (mass $< \sim 0.1 \text{ pg C}$) and realistic diameters, the associated $\sigma(\lambda)$ and $\sigma_b(\lambda)$ are more than a factor of two and three too small, respectively. To match field data for the spectral dependence of σ_b and σ_b^* as well as their magnitude at 550 nm requires unreason-

ably large disk diameters. The strong dependence of $\sigma_b(\lambda)$ on morphology shown in the computations, even for the simple disklike models, implies to us that modeling backscattering from marine particles, with their complex shapes, will be very difficult, if not impossible. Indeed, when structures such as those shown in Fig. 1 are approximated by smooth shapes (i.e., disks, washers, and so on), one must wonder about the importance of having filled the small voids with material. This could be particularly important when the voids are not randomly distributed. The strong dependence on morphology further suggests that, for backscattering, modeling disklike particles as spheres is not a realistic exercise. The volume-equivalent sphere model does not capture the spectral variation of backscattering of any of the disklike models. However, because it does provide the correct order of magnitude for σ and σ_b , particle morphology will likely not resolve the question concerning the origin of the observed backscattering in natural waters.

The primary goal of this paper, studying the efficacy of nonsphere models, and the secondary goal, studying the influence of particle morphology, have been accomplished. A simple computation of σ_b from disklike structures (i.e., approximating it with Σ_b) was developed. It performed well and was used to understand and to extend the DDA computations. The goal of using these models to extrapolate the measurements of σ_b from the visible into the red-near infrared for remote sensing has not been realized. None of our models have been able to reproduce the observed spectral dependence of both σ_b and σ_b^* in the visible, and remain consistent with estimates of coccolith diameter and mass.

References

- AAS, E. 1981. The refractive index of phytoplankton. Inst. Rep. Ser. Univ. Oslo **46**: 61.
- . 1984. Influence of shape and structure on light scattering by marine particles. Inst. Rep. Ser. Univ. Oslo **53**: 112.
- BALCH, W., P. HOLLIGAN, S. ACKLESON, AND K. VOSS. 1991. Biological and optical properties of mesoscale coccolithophore blooms in the Gulf of Maine. Limnol. Oceanogr. **36**: 629–643 (Errata: Limnol. Oceanogr. **36**: 1462).
- , K. KILPATRICK, P. M. HOLLIGAN, D. HARBOUR, AND E. FERNANDEZ. 1996. The 1991 coccolithophore bloom in the central north Atlantic II: Relating optics to coccolith concentration, Limnol. Oceanogr. **41**: 1684–1696.
- , D. T. DRAPEAU, T. L. CUCCI, AND R. D. VAILLANCOURT. 1999. Optical backscattering by calcifying algae: Separating the contribution of particulate inorganic and organic carbon fractions, J. Geophys. Res. **104C**: 1541–1558.
- , ———, J. FRITZ, B. BOWLER, AND J. NOLAN. 2001. Optical backscattering in the Arabian Sea—Continuous underway measurements of particulate inorganic and organic carbon, Deep-Sea Res. I. In press.
- BEARDSLEY, G. F., JR., H. PAK, AND K. L. CARDER. 1970. Light scattering and suspended particles in the eastern equatorial Pacific Ocean. J. Geophys. Res. **75**: 2837–2845.
- BOHREN, C. F., AND D. R. HUFFMAN. 1983. Absorption and scattering of light by small particles. Wiley.
- BORN, M., AND E. WOLF. 1980. Principles of optics. Pergamon.
- BRICAUD, A., AND A. MOREL. 1986. Light attenuation and scattering by phytoplanktonic cells: A theoretical modeling. Appl. Opt. **25**: 571–580.
- BROWN, O. B., AND H. R. GORDON. 1974. The size-refractive index

- distribution of clear coastal water particulates from light scattering. *Appl. Opt.* **13**: 2874–2881.
- BURT, W. V. 1956. A light scattering diagram. *J. Mar. Res.* **15**: 76–80.
- CARDER, K. L., R. D. TOMLINSON, AND G. F. BEARDSLEY, JR. 1972. *Limnol. Oceanogr.* **17**: 833–839.
- DRAINE, B. T. 1988. The discrete-dipole approximation and its application to interstellar graphite grains. *Astrophys. J.* **333**: 848–872.
- . 2000. The discrete-dipole approximation for light scattering by irregular targets, p. 131–145. *In* M. I. Mishchenko, J. W. Hovenier, and L. D. Travis [eds.], *Light scattering by nonspherical particles*. Academic.
- , AND P. FLATAU. 1994. Discrete-dipole approximation for scattering calculations. *J. Opt. Soc. Am. A* **11**: 1491–1499.
- GORDON, H. R., AND O. B. BROWN. 1972. A theoretical model of light scattering by Sargasso Sea particulates. *Limnol. Oceanogr.* **17**: 826–832.
- , AND A. Y. MOREL. 1983. Remote assessment of ocean color for interpretation of satellite visible imagery: A review. Springer-Verlag.
- , O. B. BROWN, R. H. EVANS, J. W. BROWN, R. C. SMITH, K. S. BAKER, AND D. K. CLARK. 1988. A semi-analytic radiance model of ocean color. *J. Geophys. Res.* **93D**: 10,909–10,924.
- , G. C. BOYNTON, W. M. BALCH, S. B. GROOM, D. S. HARBOUR, AND T. J. SMYTH. 2001. Retrieval of coccolithophore calcite concentration from SeaWiFS imagery. *Geophys. Res. Lett.* **28**: 1587–1590.
- HOLLIGAN, P., M. VOILLER, D. S. HARBOUR, P. CAMUS, AND M. CHAMPAGNE-PHILIPPE. 1983. Satellite and ship studies of coccolithophore production along a continental shelf edge. *Nature* **304**: 339–342.
- KULLENBERG, G. 1974. Observed and computed scattering functions, 25–49. *In* N. G. Jerlov and E. Steemann Nielsen [eds.], *Optical aspects of oceanography*. Academic Press.
- LINSCHOOTEN, C., AND OTHERS. 1991. Role of light–dark cycle and medium composition on the production of coccoliths by *Emiliania huxleyi* (Haptophyceae). *J. Phycol.* **27**: 82–86.
- MISHCHENKO, M. I., AND L. D. TRAVIS. 1994. Light scattering by polydispersions of randomly oriented spheroids with sizes comparable to the wavelength of observation. *Appl. Opt.* **33**: 309–324.
- , AND ———. 1998. Capabilities and limitations of a current FORTRAN implementation of the T-Matrix method for randomly oriented, rotationally symmetric scatterers. *J. Quant. Spectroscop. Radiat. Transfer* **60**: 7206–7225.
- , J. W. HOVENIER, AND L. D. TRAVIS. [ED.] 2000. *Light scattering by nonspherical particles*. Academic.
- MOREL, A. 1973. Diffusion de la lumiere par les eaux de mer. Resultats experimentaux et approche theorique. AGARD lecture series 61. Optics of the sea (interface and in-water transmission and imaging). NATO.
- . 1994. Optics from the single cell to the mesoscale, p. 93–106. *In* R. W. Spinrad, K. L. Carder, and M. J. Perry [eds.], *Ocean optics*. Oxford.
- , AND A. BRICAUD. 1981. Theoretical results concerning light absorption in a discrete medium, and application to specific absorption of phytoplankton. *Deep-Sea Res. I.* **28A**: 1375–1393.
- MUGNAI, A., AND W. J. WISCOMBE. 1989. Scattering from nonspherical Chebyshev particles. 3: Variability in angular scattering patterns. *Appl. Opt.* **28**: 3061–3073.
- PAASCHE, E. 1962. Coccolith formation. *Nature* **193**: 1094–1095.
- PURCELL, E. M., AND C. R. PENNYPACKER. 1973. Scattering and absorption of light by nonspherical dielectric grains. *Astrophys. J.* **186**: 705–714.
- STRAMSKI, D., AND D. A. KIEFER. 1991. Light scattering by microorganisms in the open ocean. *Prog. Oceanogr.* **28**: 343–383.
- VAN DE HULST, H. C. 1957. *Light scattering by small particles*. Wiley.
- VOLTEN, H., AND OTHERS. 1998. Laboratory measurements of angular distributions of light scattered by phytoplankton and silt. *Limnol. Oceanogr.* **43**: 1180–1197.
- VOSS, K. J., W. M. BALCH, AND K. A. KILPATRICK. 1998. Scattering and attenuation properties of *Emiliania huxleyi* cells and their detached coccoliths. *Limnol. Oceanogr.* **43**: 870–876.
- YOUNG, J. R., J. M. DIDYMUS, P. R. BROWN, B. PRINS, AND S. MANN. 1992. Crystal assembly and phylogenetic evolution in heterococcoliths. *Nature* **356**: 516–518.
- ZANEVELD, J. R. V., AND J. C. KITCHEN. 1995. The variation in the inherent optical properties of phytoplankton near an absorption peak as determined by various models of cell structure. *J. Geophys. Res.* **100C**: 13,309–13,320.
- ZHANG, X., M. LEWIS, AND B. JOHNSON. 1998. Influence of bubbles on light scattering in the ocean. *Appl. Opt.* **37**: 6525–6536.

Received: 26 September 2000

Accepted: 18 May 2001

Amended: 25 May 2001